Comparison of LDH-Organic/Inorganic Compound Modified Materials as Adsorbents for Heavy Metal Adsorption: Characteristic Structure and Adsorption Mechanism

Normah Normah[1], Aldes Lesbani[2*]

[1]Departement of Chemistry, Universitas Indo Global Mandiri, Palembang 30129, Indonesia
[2]Master Program of Material Science, Universitas Sriwijaya, Palembang 30139, Indonesia

Abstract

This study modified layered double hydroxide (LDH) with organic compounds in hydrochar made from rambutan peels (prepared by hydrothermal method) and polyoxometalate compounds (tipe Keggin $K_4[\alpha\text{-}SiW_{12}O_{40}].nH_2O$ compound and prepared by sol-gel method). The synthesis of modified material was conducted through the coprecipitation method. The material was then applied as an adsorbent for Fe^{2+} ions. The material's properties were analyzed using XRD (X-ray diffraction), FT-IR (Fourier-transform infrared spectroscopy), and BET surface area analysis. The physicochemical characteristics of the modified material, a combination of the pure LDH and hydrochar/polyoxometalate compounds, will influence the adsorption results of Fe^{2+} metal ions. Furthermore, its application as an adsorbent was analyzed through kinetic and isotherm parameters, which were found to follow the pseudo-first-order (PFO) and Freundlich models. The adsorption capacities for NiAl-LDH, NiAl-LDH/Hc (modified with Hc), and NiAl-LDH/POM (modified with POM) materials were 32.789 mg/g, 47.393 mg/g, and 90.091 mg/g, respectively. It can be concluded that the adsorption process occurs via physisorption, forming multilayer adsorbates at the adsorbents active sites.

1. Introduction

LDH, or Layered Double Hydroxide, is a type of 2D layered material similar to hydrotalcite, which exhibits prominent properties with unique and promising characteristics. Generally, LDH has a structure resembling brucite, with metal cations as the central atoms in octahedral layers, with their edges consisting of hydroxides as ligands [1–3]. LDH consists of positively charged metal hydroxides (trivalent and divalent metals) arranged repeatedly with anions as charge balancers between layers (such as nitrate, carbonate, sulfate, chloride, etc.) [4–7].

LDH possesses unique characteristics, including simplicity in synthesis processes, non-toxicity, and low production costs [8,9]. LDH, as a representative of 2D layered materials, has been a subject of extensive exploration in various application fields. Research and literature have detailed various LDH applications, including in medical fields (drug carriers, tissue engineering, pharmacy, cosmetics, biosensing, bioimaging, and gene delivery), energy storage (batteries and supercapacitors), and water remediation [10–15].

LDH has proven beneficial in addressing wastewater issues and environmental conservation efforts. Its usage encompasses various techniques, such as pollutant adsorption, catalysis, ion exchange, and photocatalysis, to eliminate pollutants from water [16–21]. Because

of its unique structure, LDH has become a very suitable choice as a material for improving water quality. Current water quality is vulnerable to contaminants caused by human activities such as industrial operations and household waste. Iron (Fe) is one of the many contaminants that can be harmful to health if consumed over a long period.

Fe^{2+} (ferrous iron) is a contaminant of concern due to its solubility, mobility, and redox behaviour. Its redox properties and low solubility of Fe^{2+} allow for the formation of precipitates [22]. Iron precipitates will clog water systems, inhibit fish respiration, and endanger aquatic life. The solubility of Fe^{2+} is pH dependent, remaining soluble in acidic conditions (pH = 6.7) but precipitating at higher pH levels, posing a risk in environments with fluctuating pH [23,24]. Excessive levels of Fe^{2+} can be toxic, disrupting biological processes in plants and damaging the ecological environment. High levels of Fe^{2+} also degrade water quality, causing discolouration and a metallic taste that are significant problems for domestic water users [25,26].

According to Zubair *et al.* [27], LDH modification with doping methods, particularly SA/MgFe-LDH, successfully achieved an absorption capacity of 2.42 mmol/g for As(III) and 1.60 mmol/g for As(V). For comparison, pure MgFe LDH only achieved an absorption capacity of 1.56 for As(III) and 1.31 mmol/g for As(V). This is due to the increased pore characteristics and active site numbers on LDH layers after the modification process. Based on research by Brahma and Saika [28], the ZrO_2/MgAl-LDH mixture successfully removed congo red dye with an efficiency of 97.19% and a maximum capacity of 169.42 mg. Furthermore, this adsorbent material can be reused for up to five usage cycles. Therefore, this research confirms that the potential of modified LDH development is highly effective in water remediation efforts.

The distinctive features of LDH structure include the ability to control surface chemical properties, excellent crystallinity, high specific surface area, optimal performance, ion exchange capability, memory effect, and customizable composition and structure according to needs [29–31]. Various research studies are underway regarding developing LDH modification methods to enhance its structure and performance. From these studies, it can be concluded that LDH modification methods generally involve several approaches, including intercalation researched by Huang *et al.* [32], composite material formation developed by Quang *et al.* [33], cation doping, and exploitation in representing LDH modification development strategies. The diversity of modification methods leads to the development of varied LDH compositions and structures, making it essential to understand the interaction between LDH layers and inserted guest species, whether inorganic or organic molecules, more deeply [34–36].

This research encompasses intriguing supporting materials for LDH modification development. Modification of LDH with organic compounds was reported in the study by Jiang *et al.* [20] researched LDH/loofah composite applied as a nitrate remediation solution, achieving a nitrate adsorption capacity of about 69%. In other research, Ahmad *et al.* [37] reported using Ni/Al functionalized with humic acid and magnetite for malachite green adsorption, reaching an adsorption capacity of 178.571 mg/g. Furthermore, Mohadi *et al.* [20] reported that Zn/Al LDH composited with hydrochar from duku (Lansium Domesticum) peel had a specific surface area of 22.63 m²/g and a capacity of 80.64 mg/g when applied as an adsorbent for Cr(VI) metal ions. The study proved that LDH modified with hydrochar performance than before modification, with an increase of 42.19 mg/g for the material before adsorption. In comparison, Zn/Al-Hc increased to 80.64 mg/g. This is what makes the combination of LDH very important to study. Silaen *et al.* [21] reported that the intercalation of Zn/Al LDH with polyoxometalate compounds applied as Pb^{2+} metal adsorption had a specific surface area of 14.042 m²/g and produced an adsorption capacity of 74.13 mg/g. In other research, Padalkar *et al.* [14] reported using Ni-Cr-LDH intercalated with polyoxotungstate as a hybrid supercapacitor, with a capacitance retention rate of 86%. The results of this application demonstrate that the Ni-Cr-LDH-POW nanohybrid offers excellent electrochemical functionality. In a study by Zhao *et al.* [38-39], Zn-Cr LDH intercalated with $SiW_{12}O_{40}^{4-}$ anion (polyoxometalate) showed good enhancement in photocatalytic performance in carbon dioxide and water reduction-oxidation reactions. Several studies show that LDH modification with inorganic compounds has better structural morphology advantages than LDH modification with organic compounds. However, for its performance in various applications, LDH-organic modification is better.

Therefore, this study will compare the characteristics of NiAl-LDH modified using organic compounds, namely hydrocarbons (Hc) from rambutan peel, and inorganic compounds, namely polyoxometalates (POM). Modification of NiAl-LDH with hydrochar produced through hydrothermal carbonization of rambutan peel and its utilization as an iron adsorbent represents a novel approach using biomass waste. Although the modification of Keggin anion into LDH structure has been studied previously, its impact on adsorption capacity can be considered new due to significantly enhanced performance. This modification results in superior adsorption capacity and unique structural characteristics

compared to traditional materials. Highlighting these unique properties and improved performance metrics in the context of adsorption mechanisms can further strengthen the novelty of this modification. The characteristics of the material were evaluated through XRD analysis, FT-IR characterization, and N_2 adsorption-desorption isotherms (Surface area by BET). Then, to determine the performance of the modified material, it was applied in the remediation/process of Fe^{2+} heavy metal pollution.

2. Materials and Methods

2.1 Materials

Nickel(II) nitrate trihydrate ($Ni(NO_3).3H_2O$, 99.97%), Aluminum(III) nitrate nonahydrate ($Al(NO_3)_3.9H_2O$, 99.99%) were purchased from Sigma Aldrich. Hydrochloric acid (HCl) (purity = 37%) and sodium hydroxide (NaOH, 99%) sodium tungstate (Na_2WO_4, 99.99%), sodium phosphate (NaH_2PO_4, 99%), and potassium chloride (KCl, 99%) were obtained from Merck. Iron (II) tetrachloride ($FeCl_2.4H_2O$, 99.5%) and o-phenanthroline monohydrate ($C_{12}H_8N_2$, 99%) for adsorption process from LOBA Chemie. All chemicals were used without further purification. Synthesis and adsorption experiments were carried out using distilled water.

2.2 Instrumentation of Analysis

NiAl-LDH/Hc and NiAl-LDH/POM modified samples were characterized using several spectroscopic techniques to obtain information about the material's physicochemical properties. X-ray diffraction patterns were recorded with Rigaku Miniflex-6000 XRD using Cu-Kα radiation with a scan speed 10.000 deg/min. The FT-IR spectrum was analyzed with a Shimadzu Prestige-21 FT-IR spectrometer. BET analysis was carried out using Quantachrome Micromeritics ASAP version 3.01 to determine the materials surface area, pore volume, and pore diameter.

2.3. Experimentals Methods

2.3.1 Preparation of the polyoxometalate (POM) powder

Polyoxometalate compound powder is prepared by dissolving 2 grams of sodium phosphate in 100 mL of distilled water [40]. Then, 12 grams of tungstate solution, which has been dissolved in 300 mL of boiling water and concentrated HCl, is added. This mixture is then stirred for 24 hours at a temperature of 50 °C. After that, 50 grams of $KCl.nH_2O$ is added to the mixture, and it is dried at 50 °C for 5 hours.

2.3.2 Synthesis of the NiAl-LDH/POM

The NiAl-LDH/POM is a modification of LDH material with inorganic compounds in polyoxometalate type Keggin $K_4[\alpha\text{-}SiW_{12}O_{40}]\cdot nH_2O$. Keggin-type polyoxometalate powder $K_4[\alpha\text{-}SiW_{12}O_{40}]\cdot nH_2O$ was synthesized according to the method in previous literature [41]. The synthesis of NiAl-LDH/POM was carried out using the coprecipitation method. Initially, the Nickel(II) nitrate and Aluminum(III) solutions were mixed with a molar ratio 3:1, followed by adding 2 M NaOH solution until it reached pH = 10. After precipitation occurred, polyoxometalate was previously dissolved in distilled water (50 mL) and added. The mixture was left for 24 hours and supplied with N_2 gas [42]. The resulting precipitate was filtered and dried at 60 °C for 12 hours. Finally, the green product is ground using a mortar until it forms a powder.

2.3.3 Preparation of the Hydrochar (Hc) Powder

Hydrochar powder is produced using the hydrothermal carbonization method from dried and ground rambutan peel [43]. A total of 2.5 g of rambutan peel powder is placed into an autoclave, and then 50 mL of distilled water is added. The autoclave containing the sample is heated for 10 hours at a temperature of 200 °C. After the process is complete, filtration is performed to separate the filtrate and residue. The resulting residue is dried at a temperature of 100 °C for 12 hours, yielding hydrochar powder.

2.3.4 Synthesis of the NiAl-LDH/Hc

The NiAl-LDH/Hc is a modification of LDH material with organic compounds in hydrochar rambutan peel. The synthesis of the NiAl-LDH/HC was carried out using the coprecipitation method. First, the Nickel(II) nitrate and aluminum(III) solutions are mixed in a 3:1 ratio. Once homogeneous, 2 M NaOH solution was dripped slowly until the pH reached 10. The mixture was stirred for 1 hour at 80 °C. The resulting green suspension was mixed with 1 g of hydrochar powder and stirred for three days at 80 °C. The precipitate formed was then filtered and dried at 60 °C for 12 hours. Finally, the black product is ground using a mortar until it forms a powder.

2.3.5 Adsorption experiment

The experiment of iron metal adsorption was conducted using a standard solution concentration of 30 mg/L. The Adsorption Experiment was carried out to investigate the pH, temperature, contact time between the adsorbent and adsorbate, and concentration. Each experiment was performed with 30 mg of adsorbent in a 250 mL beaker, added with 30 mL

of 30 mg/L adsorbate solution, with the solution pH ranging from 2 to 10. The effect of contact time was observed at intervals of 10 minutes. The final concentration of Fe^{2+} adsorbate was calculated using UV-Vis spectrophotometry at the maximum wavelength of Fe^{2+} (510 nm). The concentration effect was explored with variations in temperature (30, 40, 50, and 60 °C) and adsorbate concentration (0-50 mg/L) mixed with 30 mg of adsorbent in separate 250 mL chemical glassware. Equation (1) calculates the maximum adsorbed amount (mg/g).

$$q_t = \frac{(C_0 - C_t)V}{m} \qquad (1)$$

Equations (2) and (3) are employed to investigate the adsorption kinetics using pseudo first-order and pseudo second-order models:

$$\ln(q_e - q_t) = \ln q_e - k_1 t \qquad (2)$$

$$\frac{t}{q_t} = \frac{1}{k_2 q e^2} + \frac{t}{q_e} \qquad (3)$$

Equations (4) and (5) are utilized to study the Langmuir and Freundlich adsorption isotherms:

$$\frac{C_e}{q_e} = \frac{C_e}{q_{max}} + \frac{1}{q_{max} K_L} \qquad (4)$$

$$K_F = \frac{q_m}{C_O^{1/n}} \qquad (5)$$

where, q_t (mg/g) represents the amount of adsorbate adsorbed at time t (min), C_0 (mg/L) denotes the initial concentration, C_t (mg/L) denotes the concentration at time t, V (L) is the volume of the solution, m (g) is the mass of the adsorbent, k_1 (min^{-1}) represents the *pseudo first-order* rate constant, k_2 (g/mg.min) represents the *pseudo second-order* rate constant, q_e (mg/g) denotes the amount of adsorbate adsorbed at equilibrium, C_e (mg/L) is the equilibrium concentration, q_{max} (mg/g) represents the maximum adsorption capacity, K_L is the Langmuir constant, K_F is the Freundlich constant, and 1/n is the heterogeneity factor [37,44].

2.3.6 Regeneration and desorption experiment

The initial process in regeneration and desorption uses the suspension resulting from adsorption, which is then dried at 60 °C for 24 hours. Once dried, the powder undergoes the desorption process using distilled water and is stirred for 2 hours. This process is repeated through two adsorption cycles.

3. Results and Discussion

3.1 Material Characterizations

The crystalline phase of pure NiAl-LDH exhibits characteristic features of LDH structure,

as depicted in Figure 1. Diffraction peaks on the crystal planes (003), (006), (012), (015), (018), (110), and (113) were identified at 2-theta values of 11.63°, 23.22°, 35.03°, 39.23°, and 61.85°, respectively. These diffraction peaks indicate the hydrotalcite-like plane nature of NiAl-LDH, as in previous research [4] and according to JCPDS No. 15-0087. A prominent diffraction peak at 10° is associated with the interlayer spacing (002) of 7.408 Å. For NiAl-LDH modified with inorganic compounds in polyoxometalates, as presented in Figure 1, The XRD pattern of NiAl-LDH/POM displays characteristic peaks of the polyoxometalate compound on the crystal planes. Newly emerged peaks at 8.15°, 11.5°, 18.70°, and 30.40° are confirmed as typical diffraction of polyoxometalate compounds as metal oxides [45].

Successful modification is also evidenced by the diffraction peak at 8.15°, corresponding to the interlayer spacing (002) of 10.84 Å, demonstrating an increased interlayer distance. Previous research also reported that the success of modifying LDH with POM can be observed from the shift in the 2-theta angle [11,46]. In the study by Hanifah *et al.* [41], Zn/Al-LDH had a diffraction peak of 10.39°. After intercalation with the anion [$PW_{12}O_{40}$], the 2-theta angle shifted to 8.61°, indicating the formation of the ZnAl-[$PW_{12}O_{40}$] composite. Figure 1 depicts the XRD spectrum of NiAl-LDH/Hc, revealing broad diffraction peaks in the 2-theta 22.90° and 35.2°, indicative of an amorphous structure. The broad diffraction pattern reflects the characteristics of hydrochar [47,48], while peaks at 11.38° and 61.60° indicate LDH characteristics. The interlayer spacing in pure NiAl-LDH is 7.408 Å. After modification, the interlayer spacing increases significantly, with NiAl-LDH/POM reaching 10.84 Å and NiAl-LDH/Hc reaching 7.77 Å. These modifications indicate that addition polyoxometalate and hydrochar influences the structural properties of the NiAl-LDH material, resulting in an expansion
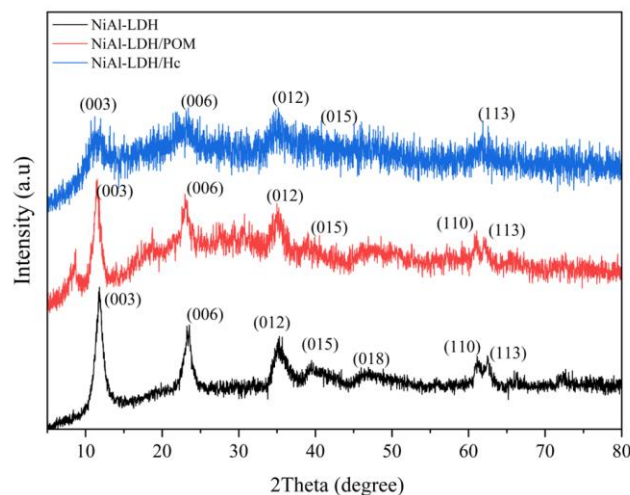

Figure 1. XRD patterns of the NiAl-LDH, NiAl-LDH/POM, and NiAl-LDH/Hc

of the distance between the layers. This change in interlayer spacing is crucial as it can affect the materials adsorption capacity and overall performance in various applications. The modification of NiAl-LDH/POM has a crystalline structure, whereas the modification of NiAl-LDH/Hc shows an amorphous structure. Broad peaks and low intensity characterize the amorphous structure due to the combined characteristics of the hydrochar compound. The amorphous structure of the material still has peaks with low intensity. These peaks are characteristic of LDH.

Figure 2 shows the FT-IR spectrum of the prepared material. The vibration band at 3483 cm^{-1} indicates the stretching mode of water molecules in the O–H group and LDH interlayers. In contrast, the weak absorption band at 1630 cm^{-1} is attributed to the bending mode of H-O-H in water molecules. The absorption band at 1370 cm^{-1} indicates the coexistence of carbonate (CO_3) and nitrate (NO_3) molecules in the LDH material gallery [49]. The FT-IR spectra of the NiAl-LDH/POM and NiAl-LDH/Hc composites show vibration patterns similar to the pristine NiAl-LDH, as seen in Figure 2. However, there are additional distinctive vibration patterns for each composite. These additions may indicate interactions between LDH and additional materials such as POM or Hc in these composites. Another low-frequency band, 617 cm^{-1}, represents the stretching of M−O, M−OH, and O-M-O bonds (where M = Ni^{2+} and Al^{3+}) [50]. Previous research also reported Hassania *et al.* [51], the characteristic peaks of the Keggin type structure at 802, 889, 964, and 1056 cm^{-1}, which correspond to the vibrations of W single bonds O single bonds W, single bonds W single bonds Ob W, double bonds W O and bonds P single O vibrations, while in this research polyoxometalate compounds exhibit characteristic absorption bands at 980 cm^{-1}, and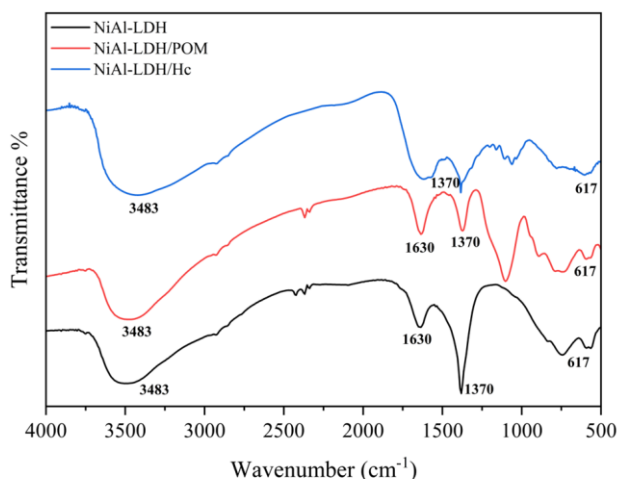 1059 cm^{-1}. Additionally, hydrochar shows characteristic absorption bands at 1059 cm^{-1} and 1044 cm^{-1} due to the C-O bond vibrations in hemicellulose [38,43].

The specific surface area and pattern of pore size distribution of the material play a significant role in the effectiveness of the adsorption process. Figure 3a illustrates the results of measurements of nitrogen adsorption and desorption parameters and an analysis of pore size distribution. The results obtained from the BET isotherm are presented in Figure 3a, with the hysteresis loop pattern classifying the material as type IV, resembling mesoporous characteristics (20-500 A) and exhibiting bottle-shaped pores.

According to Zhang *et al.* [52] and Thommes *et al.* [53], It can be observed that modified LDHs exhibit increased surface area, have more active sites, and expect to improve the adsorption performance of the adsorbate. According to the Brunauer-Emmet-Teller (BET) isotherm parameter, the specific surface area of the materials is presented in Figure 3b and Table 1. The specific surface areas of NiAl-LDH, NiAl-LDH/POM, and NiAl-LDH/Hc are 5.84 m^2/g, 98.73 m^2/g, and 46.03 m^2/g, respectively. These results show a clear trend that the increase in surface area in NiAl-LDH composites with POM or Hc is in line with the results of XRD analysis, which
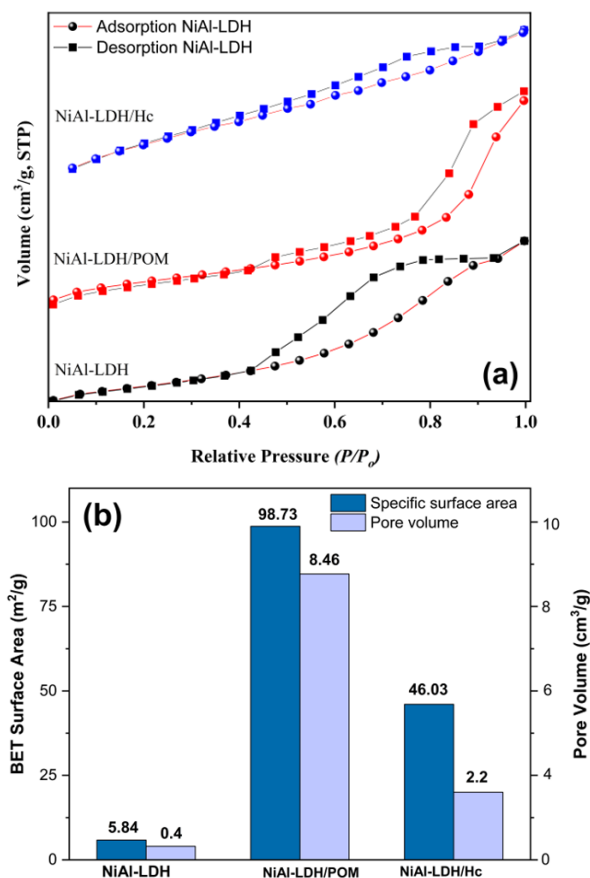

Figure 3. Isotherm of nitrogen adsorption-desorption (a) and BET surface and pore volume (b) of NiAl-LDH, NiAl-LDH/POM, and NiAl-LDH/Hc

Figure 2. FT-IR spectra (b) of the NiAl-LDH, NiAl-LDH/POM, and NiAl-LDH/Hc

shows that incorporating these materials increases the interlayer distance.

From the structural and morphological characterization results, it can be concluded that modification of NiAl-LDH with POM results in a crystalline structure. This composite mechanism increases the interlayer distance through ion exchange between POM and LDH anions. Due to its strong negative charge, POM replaces LDH anions, forming electrostatic bonds between POM and LDH groups and hydrogen bonds between hydroxyl groups on LDH and hydroxyl oxygen groups on POM [54]. Conversely, modification of NiAl-LDH with hydrochar (Hc) involves physical interactions through surface interactions. Hydroxyl groups on LDH can form hydrogen bonds with functional oxygen groups on hydrochar. Additionally, hydrochar can be intercalated between LDH layers through anion exchange, affecting the regularity of the LDH layer spacing and the specific surface area of the modified material.

3.2 Adsorption Experimental

3.2.1 Kinetic parameters

The graph depicted in Figure 4 illustrates the outcomes of the kinetics parameter concerning adsorption contact time, suggesting that as the duration of adsorption contact increases, the quantity of adsorption also rises. NiAl-LDH/POM exhibits an adsorbed Fe^{2+} amount reaching 20.408 mg/g, while NiAl-LDH/Hc reaches 9.909 mg/g, and NiAl-LDH achieves 8.025 mg/g at a contact time of 3 hours. This finding is consistent with the features observed in the analysis of the BET surface area.

An intriguing observations from Figure 4 show that NiAl-LDH/POM adsorbs Fe^{2+} ions with the highest adsorption capacity, reaching 20.408 mg/g, followed by NiAl-LDH/Hc with 9.909 mg/g, while NiAl-LDH pure 8.025 mg/g. The increase in adsorption capacity with prolonged contact duration underscores the enhancement. The improved adsorption capacity of the NiAl-LDH/POM composite material correlates with the increased surface area quality, as mentioned earlier (see Figure 3b and Table 1), notably due to the presence of POM anions. This specific combination of LDH leads to enhanced performance in Fe^{2+} ion adsorption compared to NiAl-LDH pure. Specifically, the adsorption capacity of NiAl-LDH/POM demonstrates a significant increase of approximately 2.5 fold, whereas NiAl-LDH/Hc shows an increase of about 1.2 fold.

To learn more about the adsorption process, the kinetics of adsorption analysis using *pseudo first-order* (PFO) and *pseudo second-order* (PSO) models have been elucidated by Revellame *et al.* [55], where a correlation coefficient (R^2) approaching 1 indicates that the pseudo first-order model fits the observed data (Figure 5 and Table 2). The data shows that the adsorption process for all three adsorbents fits the PFO model, as evidenced by the coefficients of determination (R^2) approaching 1. The R^2 values are 0.975 for NiAl-LDH, 0.998 for NiAl-LDH/Hc, and 0.997 for NiAl-LDH/POM. These results indicate that the adsorption of Fe^{2+} ions is predominantly governed by physisorption. The PFO model suggests that the adsorption process occurs through physical or physisorption [56]. The primary mechanism of Fe^{2+} ion adsorption involves interactions between the adsorbate and adsorbent, including electrostatic interactions, hydrophobic interactions, and active pore/site filling mechanisms [57].

3.2.2 Isotherm parameters

Isotherm parameters are analyzed using Langmuir and Freundlich models to indicate the

Table 1. The characteristics adsorbent of NiAl-LDH, NiAl-LDH/POM, and NiAl-LDH/Hc

Adsorbent	S_{BET} (m²/g)	V_p (cm³/g)
NiAl-LDH	5.84	0.4
NiAl-LDH/POM	98.73	2.2
NiAl-LDH/Hc	46.03	8.46

Tabel 2. Kinetic parameter on NiAl-LDH, NiAl-LDH/POM, and NiAl-LDH/Hc

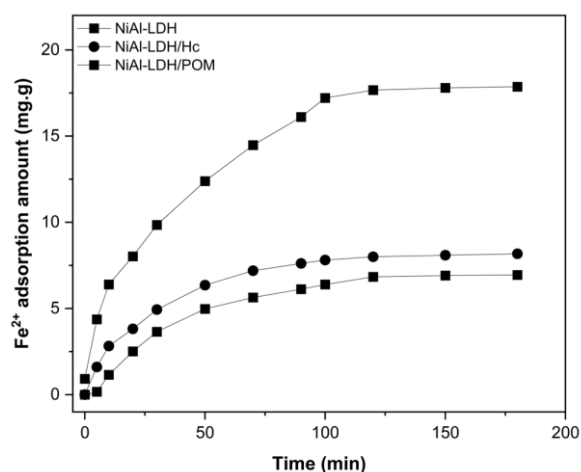| Adsorbent	Qe (mg/g)	PFO		PSO	
		K_1	R^2	K_2	R^2
NiAl-LDH	8.025	0.02	0.995	19.258	0.975
NiAl-LDH/POM	20.408	0.036	0.995	0.002	0.997
NiAl-LDH/Hc	9.909	0.0304	0.997	0.39	0.986

Figure 4. Fe^{2+} ion adsorption contact time variation curve

characteristics of the layers formed by the adsorbate on the active sites of the adsorbent. The data in Table 3 shows that the adsorption process conforms to the Freundlich model, with a correlation constant (R^2) approaching 1. The Freundlich model explains that during adsorption, the adsorbate forms a bilayer or multilayer on the active sites of the adsorbent [57].

The isotherm data presented in Table 3 indicate that the adsorption process of Fe^{2+} occurs via a *pseudo first-order* (PFO) multilayer. The adsorbent's Langmuir constant (K_L) range from 0 to 1, suggesting that the adsorption process is spontaneous. A value of $1/n > 1$ indicates heterogeneous adsorbent surfaces with adsorption processes occurring through physisorption [9]. The Freundlich constant (K_F) values indicate adsorption affinity, where higher K_F values correspond to stronger affinity of the adsorbent for the adsorbate. The maximum adsorption capacities using the Langmuir isotherm model for each NiAl-LDH, NiAl LDH/Hc, and NiAl-LDH/POM reach 32.784 mg/g, 47.393 mg/g, and 90.091 mg/g. Table 4 compares the adsorption capacity of Fe^{2+} metal ions for NiAl-LDH adsorbent, NiAl-LDH/POM, and NiAl-LDH/Hc with several other adsorbents.

There is a direct relationship between adsorption capacity data and specific surface area, which means that specific surface area significantly influences the adsorption capacity of the material. NiAl-LDH/POM has the largest surface area, at 98.73 m²/g, and adsorption capacity of 90.091 mg/g with a 2.74-fold increase. However, for the NiAl-LDH/Hc material, there was an increase of 1.44-fold. This occurs because a larger surface area provides more active sites for the adsorption process, allowing for significant interaction between Fe^{2+} ions and the material surface. Additionally, the orderly structure and presence of polyoxometalate (POM) in NiAl-LDH/POM also enhance adsorption efficiency through specific chemical interactions, such as complexation, ion exchange, and the formation of strong bonds with Fe^{2+} ions.

3.3 Regeneration of Adsorption and Desorption Process

The effectiveness of NiAl-LDH/POM in adsorbing Fe^{2+} ions is evident from the data presented in Figure 8, where the adsorbent maintains its efficiency over two cycles of use. In the second cycle, significant percentages of Fe^{2+} ions, namely 64.41%, 30.15%, and 10.87%, were adsorbed onto the material. This adsorption process primarily involves physisorption and multilayer adsorption mechanisms. Physisorption occurs as Fe^{2+} ions directly adhere to the surface of NiAl-LDH/POM via van der Waals forces, facilitated by the material's negatively charged surface, which is particularly effective at pH levels above its pH_{pzc}. As adsorption progresses, Fe^{2+} ions form additional adsorbate layers through multilayer adsorption, interacting with functional groups such as hydroxyl (-OH) and hydrogen bonds on the NiAl-LDH/POM surface. This enhances the total adsorption capacity by increasing the available surface area for interaction with Fe^{2+} ions. Subsequent desorption processes in the second cycle show significant release percentages of Fe^{2+} ions, namely 40.88%, 19.22%, and 8.71%, highlighting the adsorbent's ability to recover ions from its surface. This comprehensive mechanism underscores NiAl-LDH/POM's capability in effectively adsorbing and subsequently desorbing Fe^{2+} ions, which is crucial for wastewater treatment and environmental remediation applications.

3.4 pH_{pzc} and Adsorption Mechanism

The zero charge point (pH_{pzc}) of the material presented in Figure 6 shows that the synthesized material is at a pH of around 8, where the surface charge of the material is neutral. At this pH condition, the material operates optimally. If the

Table 4. Comparison of Fe^{2+} metal ions onto several adsorbents

Adsorbent	Q_{max} (mg/g)	Ref.
The Acid Modified Aloe vera adsorbent	45.120	[58]
Bamboo root	3.56	[59]
Burkholderia pseudomallei	49.04	[60]
Silica/lignin composite	1.1825	[61]
Pteris vittata Plant Leaves	24.367	[62]
Zn-Cr	19.426	[39]
Zn-Cr-[α-SiW12O40]	20.590	[39]
Manganese Sand	0.395	[63]
NiAl-LDH	32.784	In study
NiAl-LDH/Hc	47.393	In study
NiAl-LDH/POM	90.091	In study

Table 3. Isotherm parameters of NiAl-LDH, NiAl-LDH/POM, and NiAl- LDH/Hc

Adsorbent	Langmuir			Freundlich		
	Q_{max} (mg/g)	K_L	R^2	n	K_F	R^2
NiAl-LDH	32.784	0.069	0.922	1.647	3.121	0.997
NiAl-LDH/POM	90.091	0.002	0.834	1.197	1.744	0.994
NiAl-LDH/Hc	47.393	0.176	0.718	1.233	2.604	0.998

pH is above the pH_{pzc}, the surface charge becomes negative, significantly influencing heavy metals adsorption mechanisms. The hypothetical adsorption mechanisms for heavy metal adsorption in materials modified LDH by organic or inorganic compounds can be very diverse and complex. These mechanisms include ion exchange, surface complexation, electrostatic attraction, precipitation, intercalation, chelation, and interactions with hydroxyl groups. Due to the layered structure of LDH materials, heavy metal cations can replace anions between the layers through ion exchange. Functional groups such as -OH, -COOH, and $-NH_2$ interact with heavy metal ions, forming complexes and increasing adsorption capacity. At a pH above the pHpzc, the negatively charged surface of LDH materials enhances electrostatic attraction between the surface and positively charged heavy metal cations. This increased negative charge improves

adsorption efficiency by attracting more cations to the surface.

This study investigates the mechanisms used by the Ni/Al-LDH adsorbent to adsorb Fe^{2+} ions. As shown in Figure 7, the adsorption process of Fe^{2+} ions with Ni/Al-LDH, NiAl-LDH/POM, and NiAl-LDH/Hc involves physisorption, surface complexation reactions, and ion exchange. From the adsorption data, it can be concluded that the adsorption mechanism of Fe^{2+} ions on NiAl-LDH/POM occurs through physisorption with the formation of multilayers. The interactions in the adsorption process between Ni-Al-LDH/POM and Fe^{2+} ions are complex and encompass several critical aspects.

NiAl-LDH/POM exhibits a highly negative surface charge, especially at pH values higher than the pHpzc, allowing positively charged Fe^{2+} ions to interact electrostatically. Functional groups such as hydroxyl (-OH) on the LDH surface
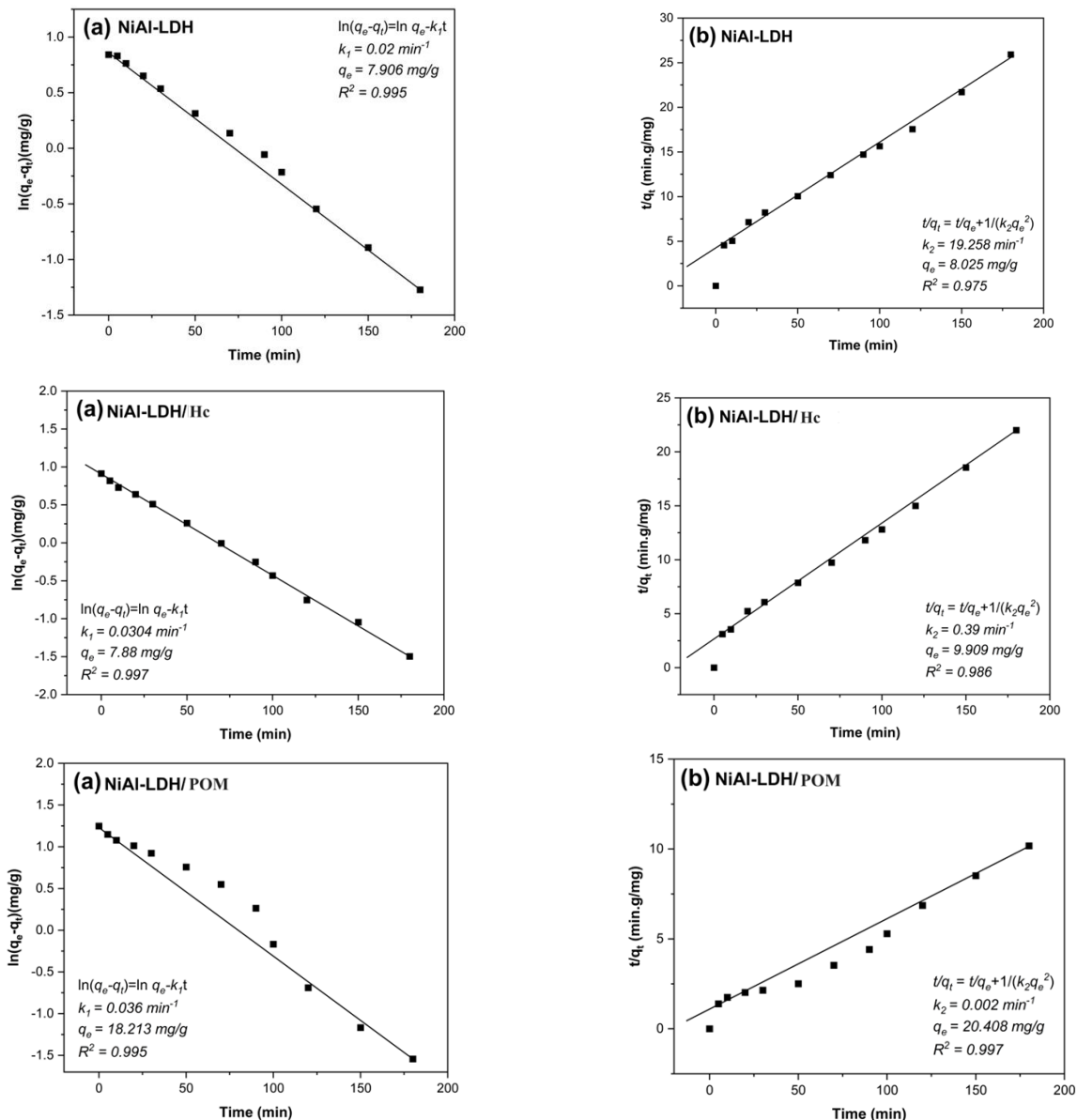

Figure 5. Kinetics curve model of Fe^{2+} adsorption process pseudo first-order (a), and pseudo second-order (b)

form complexes with Fe^{2+} ions, enhancing the materials ability to capture metal ions. Fe^{2+} ions also replace anions between LDH layers, while oxygen groups on POM form hydrogen bonds with hydroxyl groups on the LDH surface, stabilizing the adsorbed Fe^{2+} ions. The intercalation mechanism allows Fe^{2+} ions to enter the interlayer spaces of LDH. Due to the chemical properties of POM that support strong interactions with Fe^{2+} ions, these combined mechanisms result in NiAl-LDH/POM demonstrating higher adsorption capacity than NiAl-LDH/Hc.

This study has identified the adsorption mechanisms of NiAl-LDH, NiAl-LDH/POM, and NiAl-LDH/Hc using various types of data such as adsorption kinetics, adsorption isotherms, desorption, and regeneration. Additional analysis using the FT-IR method after adsorption on the utilized adsorbent is necessary to gain specific insights into these adsorption processes. FT-IR studies are required to confirm the chemical interactions between the adsorbent and Fe^{2+} ions, thereby understanding the adsorption mechanisms.
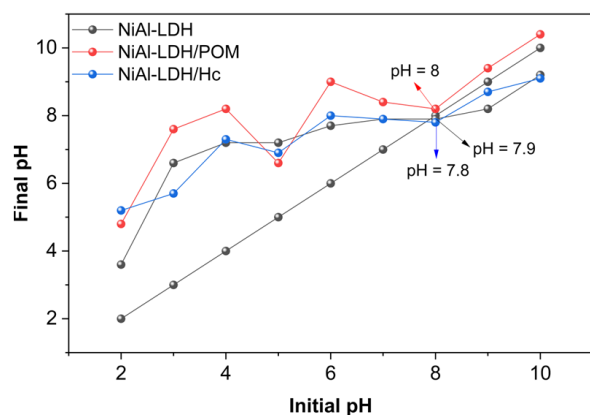
4. Conclusions

In conclusion, the modification of NiAl-LDH with polyoxometalate compounds and hydrochar (rambutan peel) resulted in NiAl-LDH/POM and NiAl-LDH/Hc, which were successfully synthesized through the coprecipitation method. Characterization using BET and XRD confirmed that modification into a composite improved the structural characteristics of LDH. Specifically, NiAl-LDH/POM showed a more significant surface area and interlayer distance than NiAl-LDH/Hc. These changes affected the increase in Fe^{2+} ion adsorption capacity. The NiAl-LDH/POM composite demonstrated an adsorption capacity of 90.091 mg/g, with a 2.74-fold increase, and 47.393 mg/g for NiAl-LDH/Hc, with a 1.44-fold increase. This underscores that modification is necessary to enhance the performance of adsorbents in adsorbing waste, and the adsorbents can be reused up to two adsorption processes. Future research should focus on developing LDH modification to improve the performance and structure of the material, as well as maintaining the regeneration stability of the adsorbent.

CRediT Author Statement

Author Contributions: N. Normah: writing-original draft, visualization, formal analysis; A. Lesbani: Writing-review, resources, conceptualization and supervision. All authors have agreed published version of the manuscript
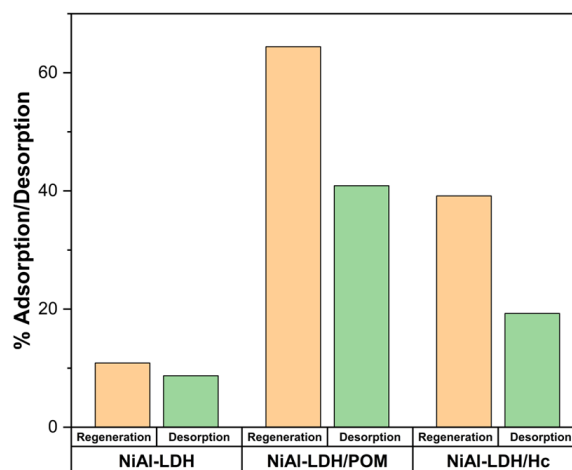

Figure 6. pH_{pzc} of NiAl-LDH, NiAl-LDH/POM, and NiAl-LDH/Hc
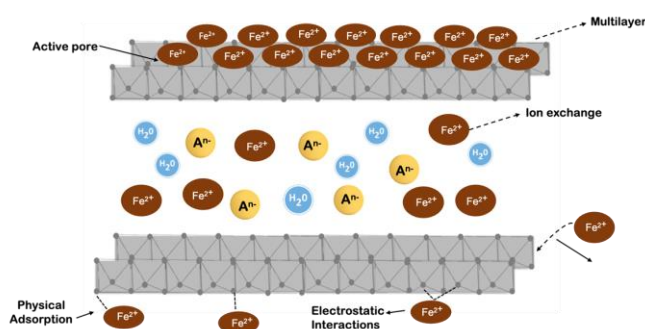
Figure 7. Ilustrasion of the Fe^{2+} ion adsorbate remediation mechanism

Figure 8. Adsorption regeneration adsorpsi and desorption

References

[1] Sekar Jeyakumar, G.F., Gunasekaran, D., Panneerselvam Manimegalai, N., Tiruchirapalli Sivagnanam, U. (2024). Tailored thymoquinone intercalated Layered Double Hydroxide (LDH) nanocomposites to accelerate mineralization for enhanced osteogenesis. *Applied Clay Science*, 252, 107339. DOI: 10.1016/j.clay.2024.107339.

[2] Chengqian, F., Wanbing, L., Yimin, D., Zhiheng, W., Yaqi, L., Ling, C., Bo, L., Siwen, Y., Junlong, W., Xianglong, D., Yue-Fei, Z., Yan, L., Li, W. (2023). Synthesis of a novel hierarchical pillared Sep@Fe$_3$O$_4$/ZnAl-LDH composite for effective anionic dyes removal. *Colloids and Surfaces A: Physicochemical and Engineering Aspects*, 663, 130921. DOI: 10.1016/j.colsurfa.2023.130921.

[3] Wang, P., Zhang, X., Zhou, B., Meng, F., Wang, Y., Wen, G. (2023). Recent advance of layered double hydroxides materials: Structure, properties, synthesis, modification and applications of wastewater treatment. *Journal of Environmental Chemical Engineering*, 11(6), 111191. DOI: 10.1016/j.jece.2023.111191.

[4] Luo, Y., Han, Y., Hua, Y., Xue, M., Yu, S., Zhang, L., Yin, Z., Li, X., Ma, X., Wu, H., Liu, T., Shen, Y., Gao, B. (2022). Step scheme nickel-aluminium layered double hydroxides/biochar heterostructure photocatalyst for synergistic adsorption and photodegradation of tetracycline. *Chemosphere*, 309, 136802. DOI: 10.1016/j.chemosphere.2022.136802.

[5] Bargmann, I., Rillig, M.C., Kruse, A., Greef, J.M., Kücke, M. (2014). Effects of hydrochar application on the dynamics of soluble nitrogen in soils and on plant availability. *Journal of Plant Nutrition and Soil Science*, 177(1), 48–58. DOI: 10.1002/jpln.201300069.

[6] Wang, R., Su, S., Ren, X., Guo, W. (2021). Polyoxometalate intercalated La-doped NiFe-LDH for efficient removal of tetracycline via peroxymonosulfate activation. *Separation and Purification Technology*, 274, 119113. DOI: 10.1016/j.seppur.2021.119113.

[7] Kobylinska, N., Puzyrnaya, L., Pshinko, G. (2022). Magnetic nanocomposites based on Zn,Al-LDH intercalated with citric and EDTA groups for the removal of U(VI) from environmental and wastewater: synergistic effect and adsorption mechanism study. *RSC Advances*, 12 (50), 32156–32172. DOI: 10.1039/D2RA05503A.

[8] Wang, Y., Zhang, L., Qiu, Z., Ren, X., Song, J., Gao, D., Guo, Q., Wang, L., Hu, X. (2024). Facile preparation of AlCo-LDH/sepiolite composites as peroxymonosulfate catalysts for efficient degradation of norfloxacin: Performance, reaction mechanism and degradation pathway. *Journal of Environmental Chemical Engineering*, 12 (2), 112231. DOI: 10.1016/j.jece.2024.112231.

[9] Kumari, S., Soni, S., Sharma, A., Kumar, S., Sharma, V., Jaswal, V.S., Bhatia, S.K., Sharma, A.K. (2024). Layered double hydroxides based composite materials and their applications in food packaging. *Applied Clay Science*, 247, 107216. DOI: 10.1016/j.clay.2023.107216.

[10] Ma, X., Zhou, L., Chen, T., Sun, P., Lv, X., Yu, H., Sun, X., Leo Liu, T. (2024). High-performance aqueous rechargeable NiCo//Zn battery with molybdate anion intercalated CoNi-LDH@CP bilayered cathode. *Journal of Colloid and Interface Science*, 658, 728–738. DOI: 10.1016/j.jcis.2023.12.102.

[11] Li, M., Chen, X., He, J., Liu, S., Tang, Y., Wen, X. (2024). Porous NiCo-LDH microspheres obtained by freeze-drying for efficient dye and Cr(VI) adsorption. *Journal of Alloys and Compounds*, 976, 173107. DOI: 10.1016/j.jallcom.2023.173107.

[12] Dan A. Lerner, Sylvie Bégu, Anne Aubert-Pouëssel, R.P., Jean-Marie Devoisselle, T.A. and D.T. (2020). Synthesis and Properties of New Multilayer Chitosan @ layered Double Hydroxide / Drug Loaded. *Materials Letters*, 1–20. DOI: 10.3390/ma13163565

[13] Bai, Y., Fang, Z., Lei, Y., Liu, L., Zhao, H., Bai, H., Fan, W., Shi, W. (2023). FCF-LDH/BiVO$_4$ with synergistic effect of physical enrichment and chemical adsorption for efficient reduction of nitrate. *Green Energy Environ*. DOI: 10.1016/j.gee.2023.05.011

[14] Padalkar, N.S., Sadavar, S. V., Shinde, R.B., Patil, A.S., Patil, U.M., Dhawale, D.S., Bulakhe, R.N., Kim, H., Im, H., Vinu, A., Lokhande, C.D., Gunjakar, J.L. (2022). Layer-by-layer nanohybrids of Ni-Cr-LDH intercalated with 0D polyoxotungstate for highly efficient hybrid supercapacitor. *Journal of Colloid and Interface Science*, 616, 548–559. DOI: 10.1016/j.jcis.2022.02.091.

[15] Liu, Y., Liu, W., Gan, X., Shang, J., Cheng, X. (2024). High-performance, stable CoNi LDH@Ni foam composite membrane with innovative peroxymonosulfate activation for 2,4-dichlorophenol destruction. *Journal of Environmental Sciences*, 141, 235–248. DOI: 10.1016/j.jes.2023.07.019.

[16] Pan, Y., Du, J., Chen, J., Lian, C., Lin, S., Yu, J. (2022). Interlayer intercalation of Li/Al-LDHs responsible for high-efficiency boron extraction. *Desalination*, 539, 115966. DOI: 10.1016/j.desal.2022.115966.

[17] Rybka, K., Hudcová, B.B., Matusik, J., Marzec, M. (2023). Interaction of vanadates with Mg/Al and Mg/Fe LDH intercalated with carbonates and sulphates based on experimental data and surface complexation modelling. *Applied Clay Science*, 242, 107047. DOI: 10.1016/j.clay.2023.107047.

[18] Xu, M., Bi, B., Xu, B., Sun, Z., Xu, L. (2018). Polyoxometalate-intercalated ZnAlFe-layered double hydroxides for adsorbing removal and photocatalytic degradation of cationic dye. *Applied Clay Science*, 157, 86–91. DOI: 10.1016/j.clay.2018.02.023.

[19] Zhao, X., Jiang, H., Xiao, Y., Zhong, M. (2024). Synthesis of polyoxometalate-pillared Zn–Cr layered double hydroxides for photocatalytic CO_2 reduction and H_2O oxidation. *Nanoscale Advances*, 6 (4), 1241–1245. DOI: 10.1039/D3NA01024D.

[20] Jiang, Z., Liu, R., Wang, Y., Cheng, W., Chen, Y., Yu, H., Pei, Y. (2024). Synergistic effect of LDHs/loofah composites for in-situ remediation of nitrate in contaminated groundwater. *Separation and Purification Technology*, 336, 126306. DOI: 10.1016/j.seppur.2024.126306.

[21] Eltaweil, A.S., Mohamed Gaber, N., El-Subruiti, G.M., Omer, A.M. (2024). Dandelion-like Cu-Ni LDH-decorated biochar/aminated chitosan composite for boosting Fenton-like degradation of doxycycline: Insights into performance and mechanism. *Journal of Molecular Liquids*, 394, 123716. DOI: 10.1016/j.molliq.2023.123716.

[22] von der Heyden, B.P., Roychoudhury, A.N. (2015). Application, Chemical Interaction and Fate of Iron Minerals in Polluted Sediment and Soils. *Current Pollution Reports*, 1(4), 265–279. DOI: 10.1007/s40726-015-0020-2.

[23] Masindi, V., Muedi, K.L. (2018). Environmental Contamination by Heavy Metals. In: *Heavy Metals*. InTech. DOI: 10.5772/intechopen.76082.

[24] Mariadi, P.D., Kurniawan, I. (2023). Analysis of Iron and Lead Levels in Groundwater in Sub-Urban Areas of Palembang. *Sainmatika: Jurnal Ilmiah Matematika dan Ilmu Pengetahuan Alam*, 20 (1), 35–46. DOI: 10.31851/sainmatika.v20i1.10077.

[25] Rusydi, A.F., Onodera, S.I., Saito, M., Ioka, S., Maria, R., Ridwansyah, I., Delinom, R.M. (2021). Vulnerability of groundwater to iron and manganese contamination in the coastal alluvial plain of a developing Indonesian city. *SN Applied Sciences*, 3 (4), 1–12. DOI: 10.1007/s42452-021-04385-y.

[26] Liu, L., Zhang, T., Yu, X., Mkandawire, V., Ma, J., Li, X. (2022). Removal of Fe^{2+} and Mn^{2+} from Polluted Groundwater by Insoluble Humic Acid/Tourmaline Composite Particles. *Materials*, 15(9), 3130. DOI: 10.3390/ma15093130.

[27] Zubair, Y.O., Fuchida, S., Oyama, K., Tokoro, C. (2025). Morphologically controlled synthesis of MgFe-LDH using MgO and succinic acid for enhanced arsenic adsorption: Kinetics, equilibrium, and mechanism studies. *Journal of Environmental Sciences*, 148, 637–649. DOI: 10.1016/j.jes.2024.01.049.

[28] Brahma, D., Saikia, H. (2022). Synthesis of ZrO_2/MgAl-LDH composites and evaluation of its isotherm, kinetics and thermodynamic properties in the adsorption of congo red dye. *Chemical Thermodynamics and Thermal Analysis*, 7, 100067. DOI: 10.1016/j.ctta.2022.100067.

[29] Zheng, J., Fan, C., Li, X., Yang, Q., Wang, D., Duan, A., Pan, S. (2024). Efficient mineralisation and disinfection of neonicotinoid pesticides with unique ZnAl-LDH intercalation structure and synergistic effect of Cu_2O crystalline surface. *Colloids and Surfaces A: Physicochemical and Engineering Aspects*, 687, 133507. DOI: 10.1016/j.colsurfa.2024.133507.

[30] Ma, J., Hou, L., Li, P., Zhang, S., Zheng, X. (2021). Modified fruit pericarp as an effective biosorbent for removing azo dye from aqueous solution: study of adsorption properties and mechanisms. *Environmental Engineering Research*, 27 (2), 200634–0. DOI: 10.4491/eer.2020.634.

[31] Chen, M., Yuan, H., Qin, X., Wang, Y., Zheng, H., Yu, L., Cai, Y., Liu, Q., Liu, G., Li, W. (2024). Improve corrosion resistance of steel bars in simulated concrete pore solution by the addition of EDTA intercalated CaAl-LDH. *Corrosion Science*, 226, 111636. DOI: 10.1016/j.corsci.2023.111636.

[32] Huang, L., Wang, L., Wang, C., Tao, X. (2022). Effect of intercalation of flocculant on adsorption properties of ZnMgAl-LDHs. *Inorganic Chemistry Communications*, 135, 109127. DOI: 10.1016/j.inoche.2021.109127.

[33] Qian, J., Zhang, Y., Chen, Z., Du, Y., Ni, B.-J. (2023). NiCo layered double hydroxides/NiFe layered double hydroxides composite (NiCo-LDH/NiFe-LDH) towards efficient oxygen evolution in different water matrices. *Chemosphere*, 345, 140472. DOI: 10.1016/j.chemosphere.2023.140472.

[34] Chen, D., Hu, X., Yip, A.C.K., Lam, F.L.-Y. (2024). Bentonite/cerium-modified LDH composite catalyst for catalytic ozonation of high-concentration indigo carmine dye solution. *Applied Catalysis A: General*, 671, 119560. DOI: 10.1016/j.apcata.2024.119560.

[35] Liu, X., Sun, T., Sun, Y., Manshina, A., Wang, L. (2024). Polyoxometalate-based peroxidase-like nanozymes. *Nano Mater. Sci.* DOI: 10.1016/j.nanoms.2024.03.002

[36] Ding, G., Sun, C., Wang, M., Cheng, G., Liu, J., Hu, Y. (2024). Effect of different metal ratios on the synthesis, morphology and microwave absorption properties of DDM–RGO@Co1–xFex–LDH porous composites. *Inorganic Chemistry Communications*, 159 (July 2023) DOI: 10.1016/j.inoche.2023.111775.

[37] Ahmad, N., Wijaya, A., Arsyad, F.S., Royani, I., Lesbani, A. (2024). Layered double hydroxide-functionalized humic acid and magnetite by hydrothermal synthesis for optimized adsorption of malachite green. *Kuwait Journal of Science*, 51 (2), 100206. DOI: 10.1016/j.kjs.2024.100206.

[38] Zhao, Q., Zhou, R., Wang, M., Xu, H., Wang, W., Yan, Y., Liu, B., Han, J., Di, Z., Shen, H., Zhao, J. (2024). Improving the corrosion resistance of waterborne epoxy resin coating by using silane modified Ca-Al LDH filler. *International Journal of Electrochemical Science*, 19(5), 100543. DOI: 10.1016/j.ijoes.2024.100543.

[39] Oktriyanti, M., Palapa, N.R., Mohadi, R., Lesbani, A. (2020). Effective removal of iron (II) from aqueous solution by adsorption using Zn/Cr layered double hydroxides intercalated with Keggin ion. *Journal of Ecological Engineering*, 21(5), 63–71. DOI: 10.12911/22998993/122190.

[40] Hanifah, Y., Amri, A. (2023). Preparation of Layered Double Hydroxide-Polyoxometalate Based Composite. *Indonesian Journal of Material Research*, 1(2), 68–73. DOI: 10.26554/ijmr.20231210.

[41] Hanifah, Y., Mohadi, R., Mardiyanto, M., Lesbani, A. (2023). Photocatalytic Degradation of Rhodamine-B by Ni/Zn LDH Intercalated Polyoxometalate Compound. *Science and Technology Indonesia*, 8(1), 93–99. DOI: 10.26554/sti.2023.8.1.93-99.

[42] Hanifah, Y., Mohadi, R., Mardiyanto, M., Ahmad, N., Suheryanto, S., Lesbani, A. (2023). Polyoxometalate Intercalated M^{2+}/Al (M^{2+}=Ni, Mg) Layered Double Hydroxide for Degradation of Methylene Blue. *Bulletin of Chemical Reaction Engineering & Catalysis*, 18(2), 210–221. DOI: 10.9767/bcrec.17789.

[43] Normah, N., Juleanti, N., Palapa, N.R., Taher, T., Siregar, P.M.S.B.N., Wijaya, A., Lesbani, A. (2022). Hydrothermal carbonization of rambutan peel (Nephelium lappaceum L.) as a Green and low-cost adsorbent for Fe(II) removal from aqueous solutions . *Chemistry and Ecology*, (Ii), 1–17. DOI: 10.1080/02757540.2022.2040996.

[44] Waheed, T., Min, P., Din, S. ud, Ahmad, P., Khandaker, M.U., Haq, S., Al-Mugren, K.S., Rehman, F.U., Akram, B., Nazir, S. (2023). Montmorillonite modified Ni/Mg/Al ternary layered double hydroxide nanoflowers with enhanced adsorption features. *Heliyon*, 9(10), e20976. DOI: 10.1016/j.heliyon.2023.e20976.

[45] Zabat, N. (2022). Green complexation for removal of Ni^{2+} from synthetic effluents by a nanomaterial polyoxometalate. *Current Research in Green and Sustainable Chemistry*, 5 (November 2021) DOI: 10.1016/j.crgsc.2021.100243.

[46] Darvishnejad, F., Raoof, J.B., Ghani, M., Ojani, R. (2023). Keggin type phosphotungstic acid intercalated copper-chromium-layered double hydroxide reinforced porous hollow fiber as a sorbent for hollow fiber solid phase microextraction of selected chlorophenols besides their quantification via high performance liq. *Journal of Chromatography A*, 1697, 463993. DOI: 10.1016/j.chroma.2023.463993.

[47] Jung, K., Yong, S., Choi, J., Hwang, M. (2021). Synthesis of Mg – Al layered double hydroxides-functionalized hydrochar composite via an in situ one-pot hydrothermal method for arsenate and phosphate removal : Structural characterization and adsorption performance. *Chemical Engineering Journal*, 420, 129775. DOI: 10.1016/j.cej.2021.129775.

[48] Oliva, M.Á., Giraldo, D., Almodóvar, P., Martín, F., López, M.L., Pavlovic, I., Sánchez, L. (2024). Designing a NiFe-LDH/MnO$_2$ heterojunction to improve the photocatalytic activity for NOx removal under visible light. *Chemical Engineering Journal*, 489(March), 151241. DOI: 10.1016/j.cej.2024.151241.

[49] Dias, Y.R., Perez-Lopez, O.W. (2023). CO_2 methanation over Ni-Al LDH-derived catalyst with variable Ni/Al ratio. *Journal of CO_2 Utilization*, 68(September 2022), 102381. DOI: 10.1016/j.jcou.2022.102381.

[50] Zhu, D., Hai, J., Wang, L., Long, X. (2023). A study on the oxidation of toluene to benzaldehyde by air catalyzed by polyoxometalate loaded on activated carbon. *Molecular Catalysis*, 551, 113626. DOI: 10.1016/j.mcat.2023.113626.

[51] Hasannia, S., Yadollahi, B. (2015). Zn-Al LDH nanostructures pillared by Fe substituted Keggin type polyoxometalate: Synthesis, characterization and catalytic effect in green oxidation of alcohols. *Polyhedron*, 99(3), 260–265. DOI: 10.1016/j.poly.2015.08.020.

[52] Zhang, Y., Li, S., Qiu, B., Chen, S., Chen, H., Fan, X. (2024). MgAl layered double hydroxide (LDH) for promoting ammonia synthesis in non-thermal plasma: Role of surface oxygen vacancy. *Chemical Engineering and Processing - Process Intensification*, 195(July 2023), 109608. DOI: 10.1016/j.cep.2023.109608.

[53] Thommes, M., Kaneko, K., Neimark, A. V., Olivier, J.P., Rodriguez-Reinoso, F., Rouquerol, J., Sing, K.S.W. (2015). Physisorption of gases, with special reference to the evaluation of surface area and pore size distribution (IUPAC Technical Report). *Pure and Applied Chemistry*, 87(9–10), 1051–1069. DOI: 10.1515/pac-2014-1117.

[54] Li, T., Miras, H., Song, Y.-F. (2017). Polyoxometalate (POM)-Layered Double Hydroxides (LDH) Composite Materials: Design and Catalytic Applications. *Catalysts*, 7(9), 260. DOI: 10.3390/catal7090260.

[55] Revellame, E.D., Fortela, D.L., Sharp, W., Hernandez, R., Zappi, M.E. (2020). Adsorption kinetic modeling using pseudo-first order and pseudo-second order rate laws: A review. *Cleaner Engineering and Technology*, 1(October), 100032. DOI: 10.1016/j.clet.2020.100032.

[56] Guo, X., Wang, J. (2019). A general kinetic model for adsorption: Theoretical analysis and modeling. *Journal of Molecular Liquids*, 288, 111100. DOI: 10.1016/j.molliq.2019.111100.

[57] Hassan, M., Du, J., Liu, Y., Naidu, R., Zhang, J., Ahsan, M.A., Qi, F. (2022). Magnetic biochar for removal of perfluorooctane sulphonate (PFOS): Interfacial interaction and adsorption mechanism. *Environmental Technology and Innovation*, 28, 102593. DOI: 10.1016/j.eti.2022.102593.

[58] Sivalingam, S., Gopal, V. (2024). Low-cost adsorbent from biomass for removal of Fe(II) and Mn(II) for water treatment: batch and column adsorption study. *Chem. Pap.* DOI: 10.1007/s11696-024-03438-x

[59] Wulandari, M., Nofrizal, N., Sulaiman, S.A.S. (2023). a Novel Approach of Using Bamboo Root Cellulose: an Alternative for Iron(II) Removal From Wastewater. *Rasayan Journal of Chemistry*, 16 (2), 921–929. DOI: 10.31788/RJC.2023.1628307.

[60] Titah, H.S., Putera, R.I., Pratikno, H., Moesriati, A. (2020). Removal of Iron(II) by burkholderia pseudomallei in brackish environment. *Environment. Asia*, 13(1), 75–85. DOI: 10.14456/ea.2020.7.

[61] Noviyanti, A.R., Yuliyati, Y.B., Maulani, G.N., Kurnia, I. (2022). Iron (II) Removal Using Activated Silica/Lignin Composite: Kinetic and Equilibrium Studies. *Jurnal Kimia Valensi*, 8(1), 85–91. DOI: 10.15408/jkv.v8i1.22715.

[62] Khan, Q., Zahoor, M., Salman, S.M., Wahab, M., Khan, F.A., Gulfam, N., Zekker, I. (2022). Removal of Iron(II) from Effluents of Steel Mills Using Chemically Modified Pteris vittata Plant Leaves Utilizing the Idea of Phytoremediation. *Water*, 14(13), 2004. DOI: 10.3390/w14132004.

[63] Kang, H., Liu, Y., Li, D., Xu, L. (2022). Study on the Removal of Iron and Manganese from Groundwater Using Modified Manganese Sand Based on Response Surface Methodology. *Applied Sciences*, 12(22), 11798. DOI: 10.3390/app122211798.